ELASTIC FINITE-DIFFERENCE MODELING OF THE 1971 SAN FERNANDO, CALIFORNIA EARTHQUAKE

By John E. Vidale and Donald V. Helmberger

Abstract

Finite-difference seismograms calculated for the 1971 San Fernando earthquake show strong effects due to lateral variation in sediment thickness in the San Fernando valley and the Los Angeles basin. Using basin structure derived mostly from well logs and teleseismically determined source parameters, two-dimensional *SH* and *P-SV* finite-difference calculations reproduce the amplitude and duration of the strong-motion velocities recorded across the Los Angeles and San Fernando basins for the period range of 2 to 10 sec. The edges of basins nearest the seismic source show ground motion amplification up to a factor of 3 over the case without the basin and tend to convert direct shear waves into Love and Rayleigh waves that travel within the basins.

Introduction

The San Fernando earthquake of 9 February 1971 produced one of the most complete sets of strong ground records from a large thrust earthquake to date and consequently has generated a large body of seismological literature. Hanks (1975) notes that seismic moment, source dimension, radiation pattern, rupture propagation, the development and dispersion of local surface waves, and azimuthal variations in the gross geological structure will appear to have first-order significance in fashioning the amplitude and frequency content of the strong-motion waveforms. Heaton (1982), among others, has modeled some of these features, but adds that many features of the observed motions remain unexplained, and considerable uncertainty still exists regarding the faulting history of the San Fernando earthquake.

One drawback of existing studies is the inability to properly simulate the propagational effects associated with the complicated sedimentary basins in and around Los Angeles. Finite-element schemes have been used to explain some of the effect of basins on surface waves, body waves, and static deformation (Drake and Mal, 1972; McCowan et al., 1977). However, these efforts did not address the demanding task of modeling seismic profiles along paths crossing the various basin and ridge structures, as discussed qualitatively by Liu and Heaton (1984). The modeling of one such three-component profile is the subject of this study.

Strong-Motion Records

The filled triangles in Figure 1 locate three-component accelerometers that recorded the strong motions of the San Fernando earthquake along a north-south profile. Figure 2 shows the vertical, radial, and transverse velocities recorded at these stations. The accelerations were integrated to velocities by EERL (1974). We model velocities for two reasons: first, it is currently economical to model only greater than 1-sec period seismic energy to ranges of 50 to 60 km with our finite-difference scheme, and velocity but not acceleration records have these periods, and second, we have less confidence in our knowledge of the geologic structures with wavelengths shorter than a few kilometers, which primarily influence shorter period seismic waves. These records comprise profile I in Liu and Heaton (1984). The absolute timing of these records is not known, so they are lined up relative to an
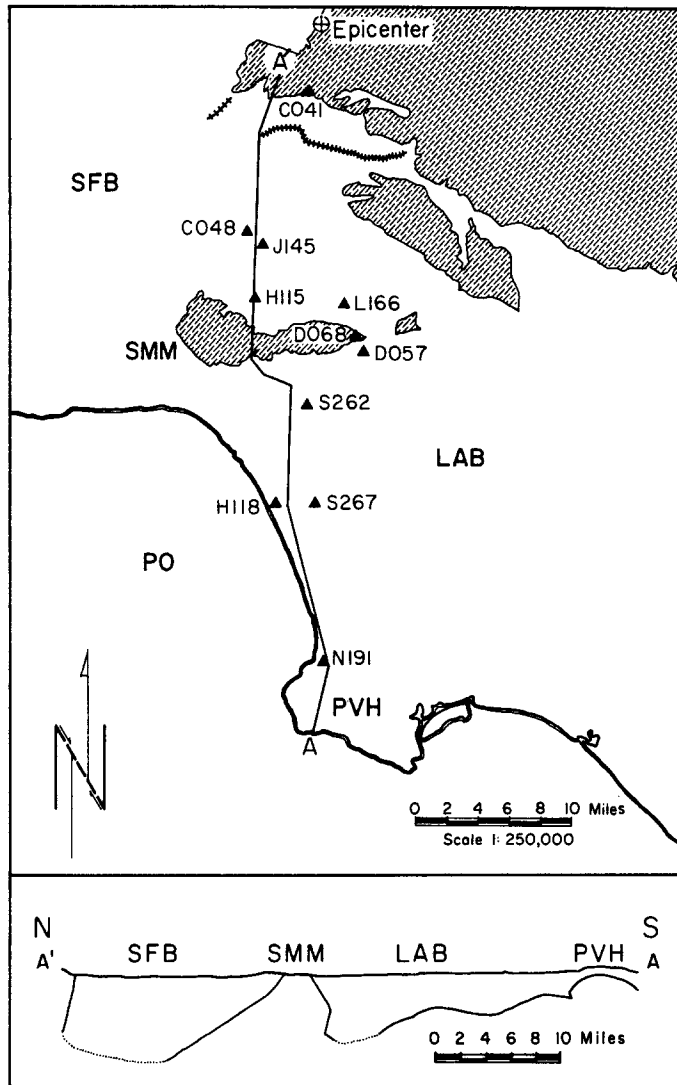
FIG. 1. Map and cross-section of the San Fernando region from Duke *et al.* (1971). The epicenter is marked by a cross. The surface breakage is indicated by the cross-hatched line. The filled triangles are the locations of the strong-motion instruments used in this section. Cross-hatched areas show surface exposure of the bedrock. The bottom of the basin for the profile A-A' is shown below, where dashed portions show where the boundary is not known. The cross-section has vertical exageration of 2:1. SFB = San Fernando basin; SMM = Santa Monica Mountains; LAB = Los Angeles basin; PVH = Palos Verdes Hills; PO = Pacific Ocean.

early, high-frequency arrival on the vertical component that is probably a direct compressional wave.

Before discussing these motions in detail, it is useful to review the geological structure along this profile. A schematic cross-section is given at the bottom of Figure 1. Figure 3 shows the geologic layering in this cross-section in more detail, with an inferred shear-wave velocity structure below. The stratigraphy is taken from Duke *et al.* (1971), who reviewed the well logs and the geological cross-sections in the literature for this area. Many well logs have been recorded around the Los Angeles basins because of oil exploration, and these logs yield estimates of density
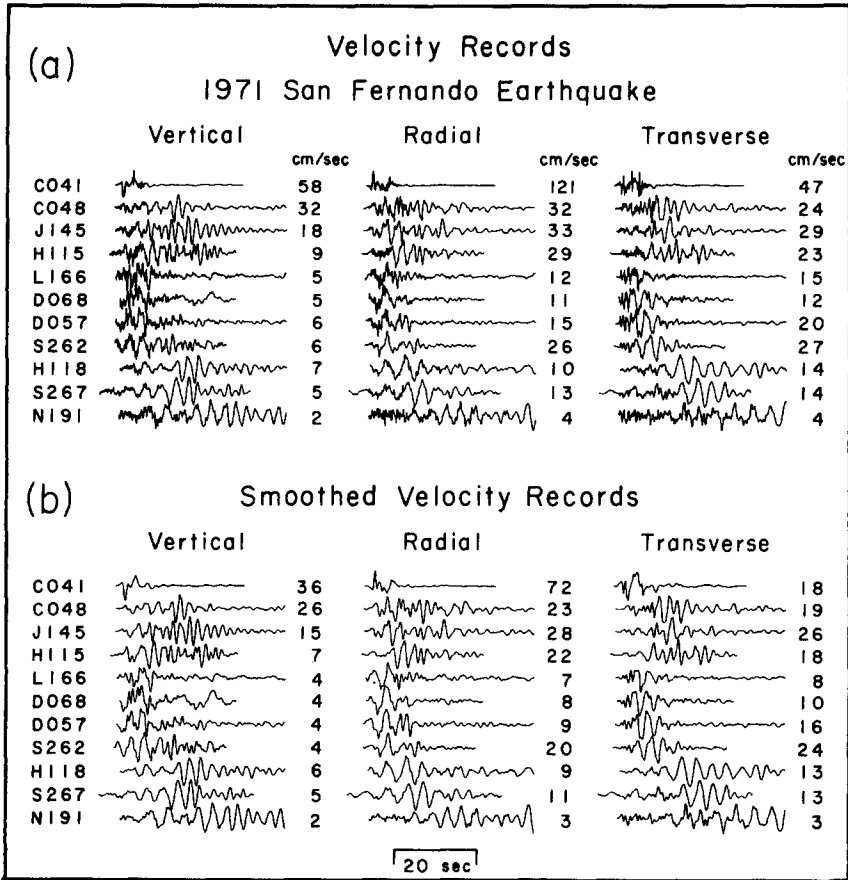
FIG. 2. (a) Velocity records of the 1971 San Fernando earthquake, taken from EERL (1974). The traces are aligned relative to a high-frequency, early arrival on the vertical component that is interpreted to be a direct compressional wave. Amplitude is given in centimeters/second. The station names are listed at the *far left*. The stations are shown in order of increasing epicentral distance, but the actual station spacing is irregular. (b) Smoothed velocity records. The records shown in (a) are convolved by a Gaussian pulse about 1 sec wide to filter out frequencies that cannot be properly handled by the finite-difference grid.

and velocity. Duke *et al.* (1971) also conducted numerous small-scale refraction surveys to find the near-surface compressional-wave velocity profile. With knowledge of the composition of the rocks at depth, the shear-wave velocity can also be reliably estimated. Near-surface values of the attenuation operator Q have also been provided by a variety of schemes. Duke *et al.* (1971) report the details of this cross-section at great length.

Although the structure within the San Fernando and Los Angeles basins along this profile can be reliably estimated from the above study, the structure below the basins is less well-known since, unfortunately, the well logs stop as soon as they encounter the basement rock. Below the basins, we use the structure given in Kanamori and Hadley (1975) for compressional waves, and assume that V_p/V_s is $\sqrt{3}$. Table 1 gives the compressional-wave velocity and density associated with each shear-wave velocity shown in Figure 3.

The motions shown in Figure 2 correspond with the geologic setting in which they were recorded. Within the San Fernando basin, a train of surface waves
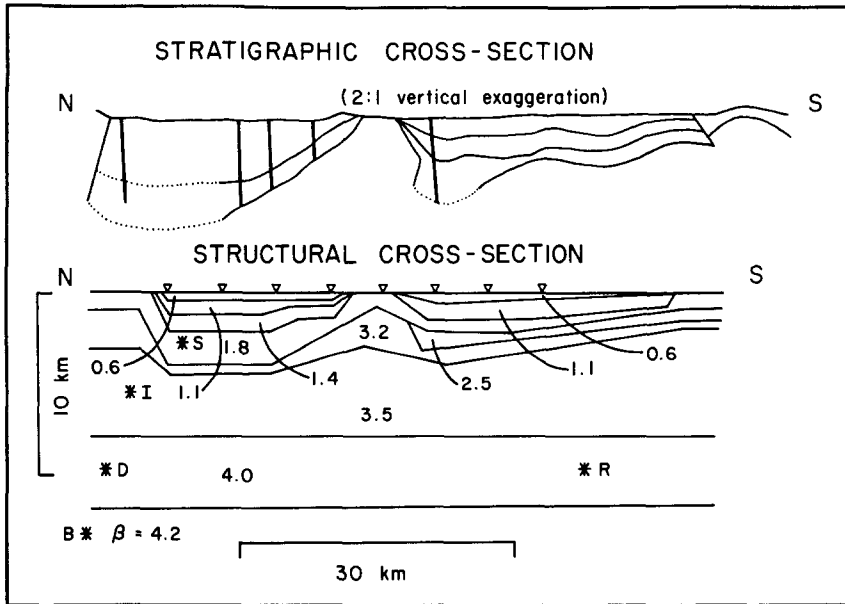
STRATIGRAPHIC CROSS-SECTION

FIG. 3. Stratigraphic and structural cross-section of the profile from the San Gabriel Mountains on the *left*, across the San Fernando basin, the Santa Monica Mountains, and the Los Angeles basin, to the Palos Verdes Hills on the *right*. The stratigraphy, the velocities, and the densities are taken from Duke *et al.* (1971), except that the velocities below the basins are taken from Kanamori and Hadley (1975). The heavy vertical lines in the stratigraphy diagram indicate the location of well logs used by Duke *et al.* (1971) to construct the model. Only the shear-wave velocity is shown; the compressional-wave velocity and the density corresponding to each shear-wave velocity are given in Table 1. The letters B, D, I, and S correspond to the locations of the bottommost, deep, intermediate, and shallow sources discussed in the text. The triangles along the surface mark the location of the receivers for the finite-difference seismograms. The vertical exaggeration is 2:1.

TABLE 1

VELOCITY AND DENSITY STRUCTURE FOR THE CROSS-SECTION IN THE MIDDLE OF THE SAN FERNANDO BASIN

P-Wave Velocity	S-Wave Velocity	Density
1.2	0.6	1.7
2.0	1.1	1.8
2.5	1.4	1.9
3.1	1.8	2.1
4.3	2.5	2.3
5.5	3.2	2.5
6.1	3.5	2.7
6.9	4.0	2.9
7.3	4.2	2.9

develops, with an apparent velocity of 1 km/sec. The wave train lengthens as it propagates across the basin. On the Santa Monica Mountains, the surface waves disappear and the amplitude falls by a factor of 2. In the Los Angeles basin, the surface wave is again present, with a slow apparent velocity, and the amplitudes increase by roughly a factor of 2 relative to the ridge. Near the ocean, in the Palos Verdes Hills, the surface wave is still present, but the amplitude has dropped more rapidly than geometric spreading would predict. Geometric spreading would be $1/\sqrt{r}$ for surface waves and $1/r$ for body waves in a whole-space. Spreading for a

layered half-space can fall off by higher powers of r for body waves, but the data suggest surface waves are present and show a decrease by a factor of 3 from H118 and S267 to N191, where the range increases from 50 to 70 km, which would require a large exponent on r. It is these patterns, some of which are discussed by Liu and Heaton (1984), that we will attempt to understand by forward modeling through the finite-difference technique with laterally varying structures.

Before forward modeling with a technique that assumes two-dimensional symmetry, we will verify that the seismic energy in the records is not significantly laterally reflected. Vidale (1986) uses complex polarization analysis that is an extension of the method of Montalbetti and Kanasewich (1970) to examine the three-component records for this profile of records from the San Fernando earthquake. Because the method works in the complex domain, elliptically as well as linearly polarized data may be interpreted. This analysis finds the direction of propagation for the Love and Rayleigh waves. The direction may be obtained because the Love wave is linearly polarized transverse to the direction of propagation, and the Rayleigh wave is elliptically polarized in the plane that contains the vertical and the propagation directions.

The analysis in Vidale (1986) shows that the energy in this particular profile is traveling within 15° of radially outward from the source. This suggests that despite the three-dimensional nature of the basins, the geometry may be approximated by a two-dimensional model with useful results. We should note, however, that although the energy in this profile travels radially out from the source to the receiver, amplitude attenuation due to geometrical spreading depends on the curvature of the wave front; so, the amplitude may vary somewhat due to three-dimensional effects, even if the energy path is not laterally deflected.

To match the frequency limitations of the finite-difference algorithm, we low-pass filter the data. The finite-difference method can only propagate energy with six or more grid points per wavelength; so, to properly treat high frequencies, more grid points and therefore more calculation is required. Figure 2b shows the filtered vertical, radial, and transverse velocities that will be addressed in this modeling study.

REVIEW OF SOURCE PARAMETERS

The San Fernando earthquake has also been the subject of studies that concentrated on other data sets, namely the teleseismic body waves, the long-period surface waves, the location of preshocks and aftershocks, and the static displacements. These studies will help us estimate the source parameters. First, we will briefly review these studies to help clarify some of the uncertainties.

The seismicity studies (Allen et al., 1973; Whitcomb et al., 1973) reveal a relatively diffuse zone of aftershocks with a combination of thrust and left-lateral strike-slip mechanisms. By locating the main shock relative to well-located aftershocks recorded on a temporarily deployed array, Whitcomb et al. (1973) place the hypocenter at a depth of 8 km at 34°24.7'N and 118°24.0'W, with the mechanism listed in Table 2. The errors in hypocentral depth are conservatively estimated at ±8 km vertically and ±4 km horizontally. The aftershocks suggest that the plane of faulting dipped 35° to the north down to 8 km depth, below which the fault plane dipped 50°. The mechanism derived from first motions by Whitcomb et al. (1973), listed in Table 2, is similar to the teleseismic results.

Examination of the static displacements due to the earthquake (Alewine, 1974) reveals distributed slip from near the surface to a depth of about 14 km along the

TABLE 2
SOURCE PARAMETERS OF THE SAN FERNANDO EARTHQUAKE

Study Method		Strike	Dip	Rake	Depth (km)	Moment (×10²⁶ dyne-cm)
Whitcomb (1973)		−67°	52°	72°	8	—
First motions						
Alewine (1974)		−67°	53°	72°	0–14	1.0–2.2
Static displacements						
Alewine (1974)		−67°	53°	66°–82°	0–15	1.7
Surface waves						
Langston (1978)	First source	−79°	44°	80°	15	0.53
Teleseismic records	Second source	−80°	18°	96°	10	0.32
Langston (1978)	First source	−70°	53°	76°	8–15	0.41
Teleseismic records	Second source	−80°	29°	90°	0–10	0.45
Heaton (1982)	First source	−70°	54°	76°	3–16	0.7
Combined study	Second source	−75°	45°	90°	0–10	1.0

north-dipping fault plane. The portion of the fault from the surface down to 5 km depth underwent about 5 m of slip, and the segment from 10 to 14 km depth shows 2 to 5 m slip; there may be an area of less slip from 5 to 10 km depth. The greater the depth, however, the worse the resolution of static analysis. The static moment is estimated to be between 1.0 and 2.2 × 10²⁶ dyne-cm.

The 16- to 60-sec fundamental Rayleigh waves generated by the San Fernando earthquake are analyzed by Alewine (1974), and given the strike and dip suggested by Whitcomb *et al.* (1973); the moment is found to be 1.7 × 10²⁶ dyne-cm. Half the moment release is found to be at depths of about 3 to 8 km, and the other half of the moment release is below about 10 km.

The teleseismic body-wave studies (Langston, 1978; Heaton, 1982) use records from long-period WWSSN stations to find the mechanism and 5- to 30-sec period faulting history in time and space.

Both Langston (1978) and Heaton (1982) find a double source. In the various models, there is a source at 10 to 15 km depth with a moment of 0.5 × 10²⁶ dyne-cm, and there is a shallower source with a shallower dip angle that also has a moment of 0.5 × 10²⁶. The two sources are found to have slightly different strikes and the shallower source dips less, as shown in Table 2. When Heaton (1982) attempts to model the near-in records and static data as well as the teleseismic data, his estimate of the total moment rises to 1.7 × 10²⁶ dyne-cm. Figure 4 summarizes the results from the teleseismic modeling of Langston (1978) and Heaton (1982).

The short-period WWSSN records are also examined in the search for higher frequency (0.5- to 3.0-sec period) details of the faulting history (Hanks, 1975; Langston, 1978). The work of both Hanks (1975) and Langston (1978) suggests that the first pulse of short-period energy originated about 12 km below the surface. If the pulse of energy came from the hypocenter, which was on the fault plane as defined by the aftershocks, the location from Whitcomb *et al.* (1973) would have to be in error by 4 km vertically and 4 km horizontally. Some of the short-period WWSSN records, however, indicate a small precursor about 2 sec before the initial large pulse; so, perhaps the hypocenter and the location of the short-period energy release are not coincident.

In this study, we find that a point source at 10 km depth with the mechanism of Heaton's deep source (which is nearly identical to Langston's deep source) can

RESULTS FROM TELESEISMIC
BODY WAVE STUDIES

Langston (1978)

Point
Sources

$M_o = 0.3 \times 10^{26}$ ... 5 km
... 10
$M_o = 0.5$ ... 15

Langston (1978)

Finite
Sources

$M_o = 0.5$ ... 5 km
... 10
$M_o = 0.4$ ... 15

Heaton (1982)

Finite
Sources
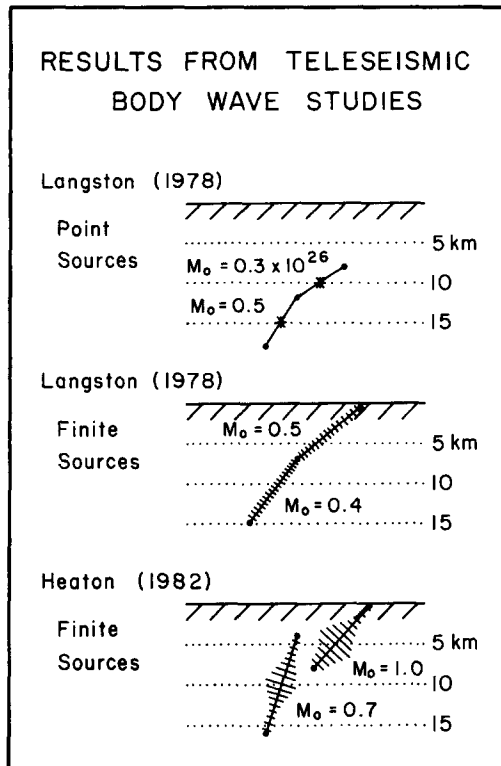
... 5 km
$M_o = 1.0$ ... 10
$M_o = 0.7$ ... 15

FIG. 4. Schematic north-south cross-section of results from teleseismic body-wave studies. Langston (1978) interprets the faulting of the San Fernando earthquake as two-point sources (*top*) and as two finite segments (*middle*). The moment is assumed to be uniformly distributed with depth for each source in the *middle trace*. Heaton (1982) combines the teleseismic data, near-field data on hard rock sites, and static data to find the two nonintersecting finite-fault segments shown in the *bottom trace*. The moment is assumed to be nonuniformly distributed with depth for each source in the *bottom trace*. Details of these models may be found in Table 2.

explain most of the data. The sensitivity of our modeling to changes in source depth and mechanism are discussed in the following section.

NUMERICAL MODELS OF THE STRONG MOTIONS

Details of these two-dimensional finite-difference SH and P-SV algorithms that are used to calculate the Green's functions are described in Vidale *et al.* (1985), Vidale and Clayton (1986), Vidale and Helmberger (1987), and Clayton and Vidale (in preparation, 1987). The finite-difference method is of fourth-order accuracy as defined by Alford *et al.* (1974). The seismic energy from the source is introduced into the grid by the method of Alterman and Karal (1968). This method, as we use it, requires the source to be placed in a region of the grid of constant density and velocities.

Expressions describing line-source excitation functions used in the line-to-point-source mapping may be found in Helmberger and Vidale (1988). The exact dislocation solution is expressed in an asymptotic series in which the displacement decouples into the SH and P-SV systems where the vertical and azimuthal radiation patterns separate explicitly. Therefore, we can make separate finite-difference calculations to model the SH and P-SV radiation. The expressions containing the

vertical radiation patterns are loaded into the grid source box. The azimuthal radiation patterns are factored in later according to the fault orientation. This finite-difference procedure does not handle the near-field terms properly at small horizontal distances, but numerical checks indicate accurate results beyond about 10 km for a source at a depth of 10 km.

The Green's functions for the transverse component of velocity for the four source locations shown in Figure 3 are displayed in Figures 5 and 6, where $j = 4$ corresponds to the strike-slip and $j = 5$ to the dip-slip components. The Green's functions correspond to the $\tilde{V}_j$ in equations (1) and (14) of Vidale et al. (1985), and are equivalent to equation (24) in Helmberger and Vidale (1988) for the case where the source is impulsive and only one of A_4 and A_5 is nonzero. A Q of 25 is included in the calculation.

The ranges indicated on the left are appropriate for the deepest source. For shallower sources, we chose to leave the receivers at the same point in the structure with the same range, rather than shift them by the difference in hypocentral position, so the ranges are approximate for the shallower sources. Note that the shallower sources are located further to the south. The change in polarity for the first station for the source S indicates that the source is just to the south of the first receiver. However, we are only interested in the records written at the larger distances where the near-field terms can be neglected. A seismic attenuation Q of
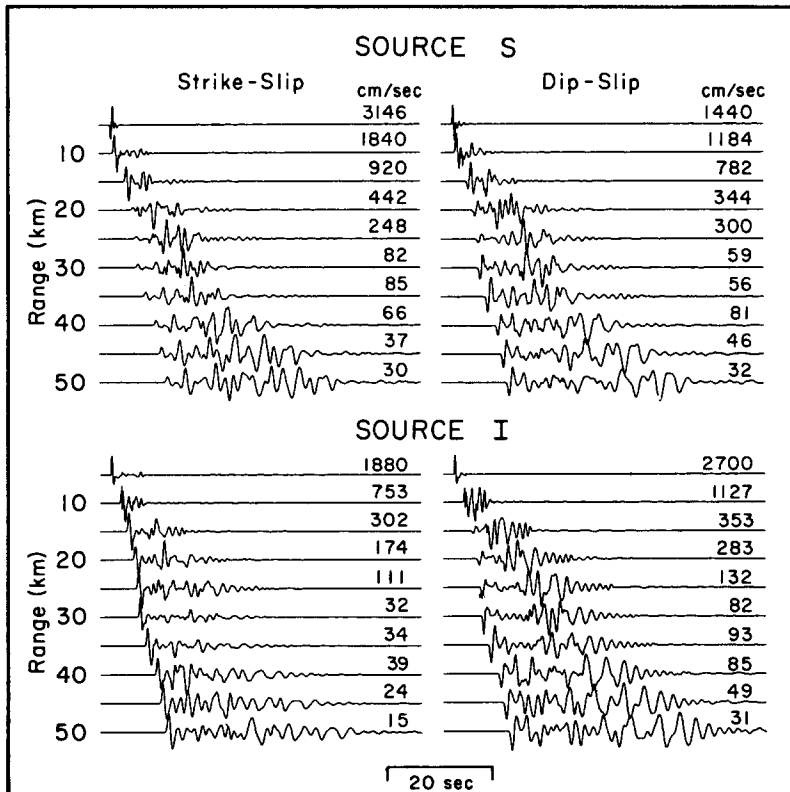

FIG. 5. Green's functions for the transverse component of velocity with S and I source locations. The strike-slip case corresponds to $A_4 = 1$ and $A_5 = 0$, and the dip-slip case corresponds to $A_4 = 0$ and $A_5 = 1$. Moment scaling is discussed in the text. The source-time function is impulsive, and the frequency content is limited by the seismic Q of 25.
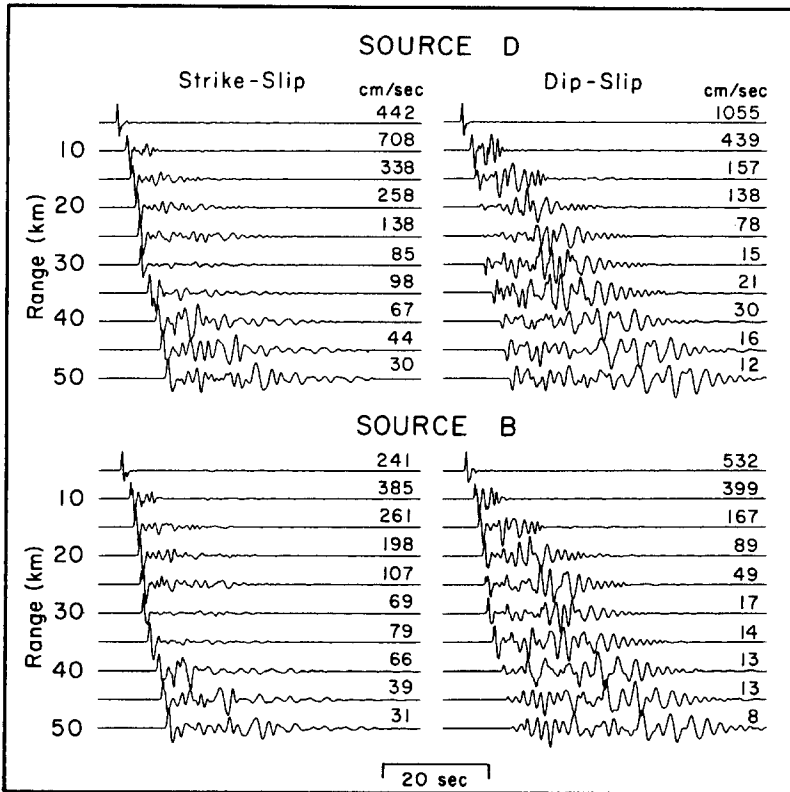
FIG. 6. Green's functions for the transverse component of velocity with the D and B source locations. The strike-slip case corresponds to $A_4 = 1$ and $A_5 = 0$, and the dip-slip case corresponds to $A_4 = 0$ and $A_5 = 1$. Moment scaling is discussed in the text. The source-time function is impulsive, and the frequency content is limited by the seismic Q of 25.

25 is assumed; this value falls within the wide range of Q's reported by Duke *et al.* (1971).

Incorporation of spatially varying attenuation into finite-difference calculations is possible with Pade approximants (Day and Minster, 1984; Witte and Richards, 1986) but requires much computation. We use a simpler scheme in this paper to include the effect of a constant Q. Our scheme is derived from one that has been used in generalized ray calculations for some years (Carpenter, 1967). The quantity $t^* = \int 1/vQ\,ds$ or $t^* = \int 1/Q\,dt$ may be computed for a given ray, and a convolutional attenuation operator can be computed for any t^* (see, e.g., Futterman, 1962). If Q is constant, $t^* = t/Q$, thus t^* is only a function of time. In the computation of teleseismic arrivals, t^* remains approximately constant during the time window in which a P wave or even several branches of a P-wave triplication arrive.

The profile in this paper is more complicated, however, in that the time window is not short compared to the travel time from the source. Since Q is included with a convolution-like operator, however, we need not use the same operator for each point in time. Q is then incorporated by convolving at each point in time of the seismograms the Futterman Q operator for a $t^* = t/Q$. Of course, the convolution-like operation may not be done in the frequency domain since every time point requires a different Q operator. In practice, we only calculate a new Q operator for each 50 time points since the Q operator changes gradually with time, and computing an operator requires a Fast Fourier transform.

A moment of 10^{26} dyne-cm is used for the 10 km source depth. To compare amplitudes between different depths, we hold AD_0 rather than the moment μAD_0 constant to avoid the strong tendency to generate larger seismic motions in softer material.

The Love waves dominate the motions for the dip-slip case at all depths, whereas the direct S arrivals are more noticeable in the strike-slip case, especially at the greater depths. These features may be understood in terms of vertical radiation patterns. The strike-slip source radiates most of the energy horizontally, which appears as direct body waves, while the dip-slip pattern tends to radiate energy vertically, where it can be trapped to form surface waves.

The strike-slip Green's function is the most important for the transverse component of motion for the San Fernando earthquake, despite the fact that the mechanism is dominantly thrust. This is because a 45° dip-slip event produces the same radiation pattern of SH energy as a strike-slip event, but rotated 45° in strike. The A_4 coefficient (strike-slip case) is about 10 times larger than the A_5 coefficient (dip-slip case) in both Langston's (1978) and Heaton's (1982) solution for the deep source. Heaton's shallow source is also dominated by the strike-slip solution but Langston's shallow source is about one-third composed of the dip-slip solution. For these reasons, we have conducted most of our sensitivity studies with the strike-slip case. Synthetic transverse ground motions can be generated from the Green's functions shown in Figures 5 and 6 by performing the operations indicated in equation (1) of Vidale et al. (1985). Transverse velocity records convolved with the 3-sec time function shown in Figure 8c are shown in Figure 7b. Seismograms for a flat-layered approximation to the deep basin structure are included in Figure 7a for comparison.

These synthetic seismograms for a flat structure are sensitive to the source depth in both amplitude and waveform. The shallowest source excites large, slow Love waves, and would make even larger, higher frequency waves were it not for the strong damping to the Q of 25. Even considering the inefficiency of the mechanism of the shallow source in exciting radiation along this profile, 0.1×10^{26} dyne-cm of moment in the shallow source would suffice to generate waves as large as those observed.

The shallow source creates such large waves for two reasons. First, the softer material near the surface allows larger velocities to develop for a given moment than the stiffer material at greater depth. Second, the shallower source is closer to the edge of the slow San Fernando basin than the deeper sources, and it can trap a larger portion of its energy as surface waves. The direct body-wave has a negligible amplitude compared to the surface wave for all but the two closest stations. Source I generates smaller seismic waves and excites surface waves with a range of velocities. The direct arrival is distinct for all ranges, and source D produces predominantly a direct diving wave. Surface waves do not contribute much energy to the records for the intermediate and deep sources. It is clear that, for this flat-layered geometry, the shallow source generates much more surface motion per unit moment than the intermediate and deep sources.

The moments of 1 to 2×10^{26} dyne-cm found by the studies in Table 2, placed at the intermediate or deep depth are consistent with the peak velocities observed. The synthetic waveform fit with the data, however, is improved considerably by the empirical source-time function described below.

The waveforms from the more realistic structure, Figure 7b, are more complicated than in the flat-layered case. Sources at all depths can excite noticeable surface
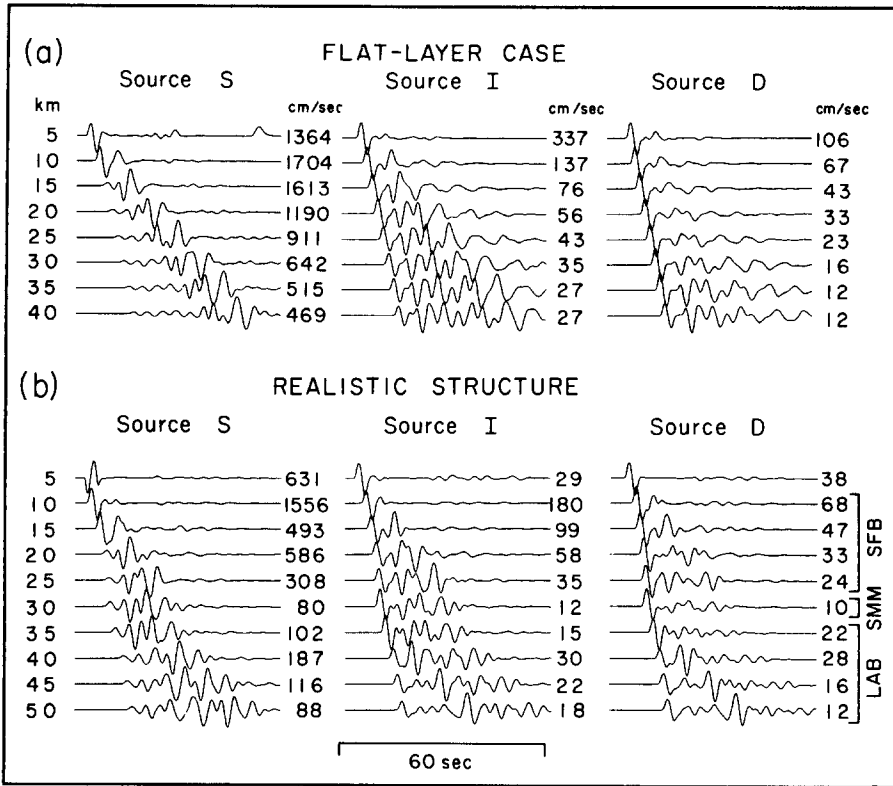
FIG. 7. (a) Finite-difference seismograms for the transverse component of velocity for the model with flat layers of the thickness and velocities appropriate for the middle of the San Fernando basin in Figure 3, listed in Table 1. The source has a Gaussian time function 3.0 sec in width that is shown in Figure 8c. The mechanism is strike-slip, and the moment scaling is discussed in the text. Velocities are in centimeters/second. (b) Finite-difference velocity seismograms for the model shown in Figure 3. The source has the same time function 3.0 sec in width as (a). The mechanism is strike-slip. The location of the shallow, intermediate, and deep depth sources are indicated in Figure 3.

waves in both basins. This result arises because direct energy incident on the edges of the basin can be trapped by the basins much more efficiently than the direct waves can tunnel into the flat layers (see, e.g., Vidale et al., 1985). The source S still excites larger motions on the surface, again largely because a source in the slower medium generates larger amplitude waves and also because the shallow source is closer to the basin edge, allowing a larger percentage of its energy to be trapped. A source at location B produces seismograms very similar to those of a source at location D, except for a smaller amplitude, which is due to the faster velocity at the deeper depth.

The surface waves that are traveling within the San Fernando basin can, to some extent, tunnel across the Santa Monica Mountains to enter the Los Angeles basin. Significant energy also must be reradiated as body-wave energy when the surface waves reach the far side of the basins, since the surface waves do not either continue into the next basin or reflect back from the edge. Little energy reverses direction and travels back to the north in the basins. The peak amplitudes of the velocity traces are greater for the realistic structure than for the flat-layered structure in the San Fernando basin, but the reverse is true in the Santa Monica Mountains. In the Los Angeles basin, the peak amplitudes are less than in the flat-layered case because the receivers are in the shadow of the mountains, for the case of sources S

and I. Source D, however, excites the Los Angeles basin with a direct S wave, which is more efficiently converted to surface waves in the realistic rather than the flat-layered geometry.

Note that the seismograms for the source D in Figure 6 show many of the characteristics of the data displayed in Figure 2; i.e., reduced amplitude with simple direct pulses at the Santa Monica Mountains and significant surface-wave arrivals in each basin. Source I, at 6 km depth, matches the data nearly as well, but has too much energy in surface waves compared to direct waves. For the rest of the paper, we will consider only a point dislocation source at 10 km depth. Most probably, the source was actually finite, but most of the effect of source finiteness may be included in the source-time function for the purpose of understanding the motions in the basins. What we do not include seems less significant than the effect of the structure, which is the focus of this paper. This conclusion is justified by noting that a point source with an empirical source-time function, an independent velocity structure, and a teleseismically determined mechanism explains most of the velocity records observed in the basin. This approach introduces a slight contradiction; we put both pulses at 10 km depth with the same mechanism, while Langston (1978) and Heaton (1982) separate the two pulses and give them distinct mechanisms. Either the separation and differing mechanisms are less than were estimated or our simpler approach produces a similar result; for in the end, we can match the data within the limitations of our knowledge of the structure and our two-dimensional approach.

The finite-difference seismograms in Figure 7b suggest that the body wave appears at the ridge with a time function very similar to the source-time function. The waveform of the transverse component at the ridge station D068 is shown in velocity and displacement in Figure 8. The displacement trace shows too strong pulses of
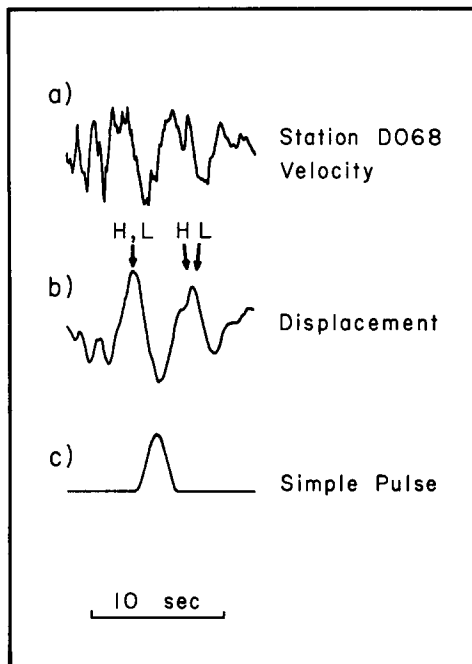

FIG. 8. The calculation of an empirical source-time function for the deep source. (a) The observed transverse velocity waveform at the Santa Monica Mountains station D068. (b) The displacement waveform at station D068. Predictions of secondary arrivals by Langston (1978) and Heaton (1982) are indicated by the H and L above the trace. (c) The Gaussian time function assumed in the construction of the synthetics shown in Figure 7.

energy. Heaton's (1982) source model predicts a strong second arrival with a 4-sec time delay, while Langston (1978) finds a value of 4.9 sec. Both models appear to fit the observations at the ridge quite well. The relative amplitude ratio of the two pulses appear to favor the Langston source model, which is given in Table 2.

One possible strategy at this point would be to add the secondary source and make adjustments in the source-time description. Another approach that might be called an "empirical source model" is to assume that the displacement record D068 is a good source description in this particular direction and use it to predict the other seismograms. This empirical approach is adopted and the finite-difference seismograms with the empirical source model are presented in Figure 9. The moment, which is difficult to control because the long-period information is absent from the data, is set so that the amplitude of the observed transverse record at station D068 matches the synthetic at that range. When a cluster of stations are at nearly the same range, only one representative trace is plotted.

In Figure 9, the agreement between the data and the finite-difference seismograms is excellent at all but the closest range, C041 at Pacoima Dam, where the near-field assumptions break down and finiteness and directivity may become important. The frequency content of the records in the San Fernando valley is higher in the data
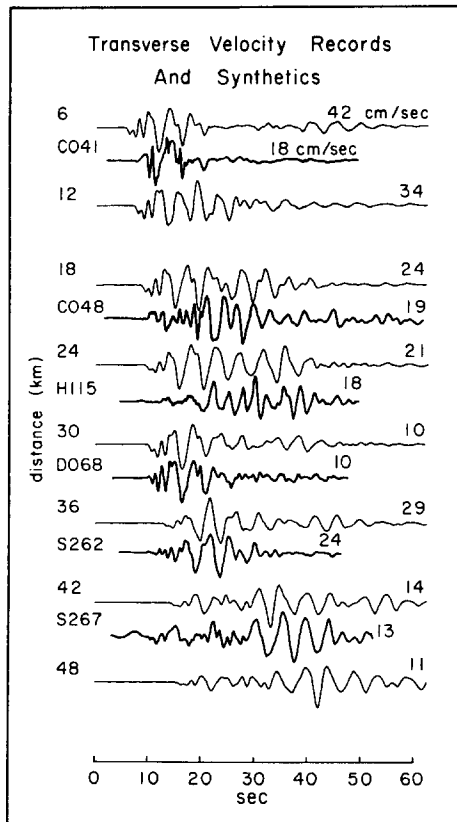

FIG. 9. Comparison of filtered transverse component of data with finite-difference seismograms computed with the empirical time function shown in Figure 8. The heavy traces show the data, with the station name to the *left* and the amplitude in centimeters/second to the *right*. The light traces show the finite-difference seismograms, with the range in kilometers to the *left* and the amplitude to the *right*. The finite-difference seismograms assume point source D in the structure shown in Figure 3 and a Q of 25. The source-time function is chosen, and the source amplitude is scaled so that the waveform and amplitude of the synthetic seismogram at the ridge station (30 km) match that of station D068.

than in the synthetics, which is probably due to inaccuracies in the velocity profile which produce too low a resonant frequency in the finite-difference modeling.

The P-SV motions can be simulated by constructing Green's functions as for the SH case, except that two rather than three fundamental fault orientations are required. These responses for the assumed two-dimensional structure and 10 km deep source are given in Figure 10. As discussed earlier, the vertical radiation patterns strongly influence the relative body-wave to surface-wave ratios. The A_1, A_2, and A_3 factors are all significant for the deep source mechanism. The A_3 or 45° dip-slip component dominates, as might be expected for a primarily thrust event, because A_3 is slightly larger than A_1 and A_2, and the amplitudes of the Green's functions for A_3 are larger than those of A_1 and A_2.

The finite-difference seismograms are compared with the data for the vertical and radial components in Figures 11 and 12. Again, when a cluster of stations are at nearly the same range, only one representative trace is plotted. The amplitude of the synthetic seismograms is determined from the SH scaling described previously. The match in timing is somewhat arbitrary, since there is no absolute timing for the data.

The match in amplitude between the P-SV synthetic velocities and the data is good. In addition, the duration of shaking in the San Fernando basin and the waveforms at the start of the record in the Los Angeles basin are also well-modeled, using the empirical time function. As in the SH case, the Santa Monica Mountains produce a strong decrease in the amplitude of the velocity traces, and both basins apparently convert the direct waves into surface waves, Rayleigh waves in this case, at the edge nearest the source.
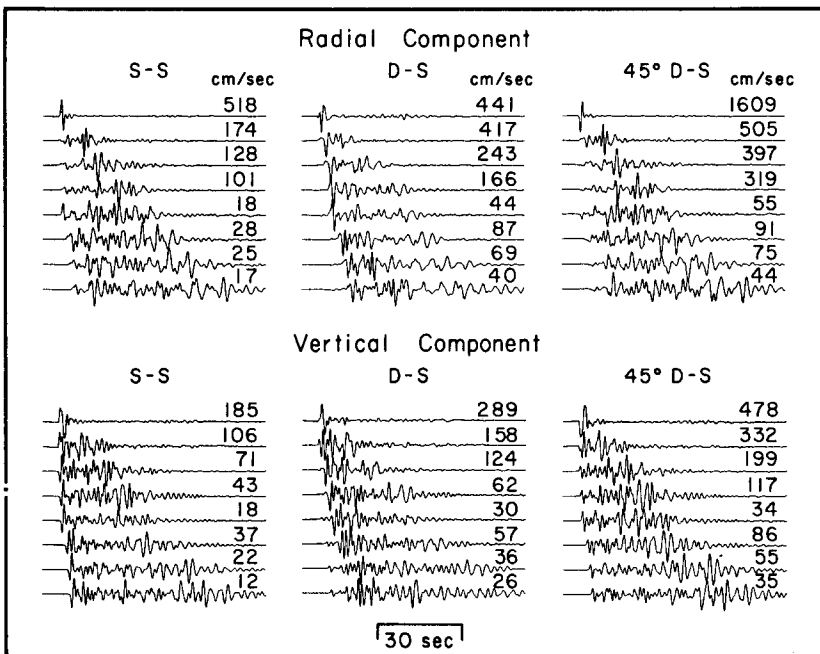

FIG. 10. Vertical and radial Green's functions for source D. The strike-slip case corresponds to $A_1 = 1$, $A_2 = 0$, and $A_3 = 0$. The dip-slip case corresponds to $A_1 = 0$, $A_2 = 1$, and $A_3 = 0$. The 45° dip-slip case corresponds to $A_1 = 0$, $A_2 = 0$, and $A_3 = 1$. The moment of each Green's function is 10^{26} dyne-cm. The frequency content is limited primarily by the seismic Q of 25.
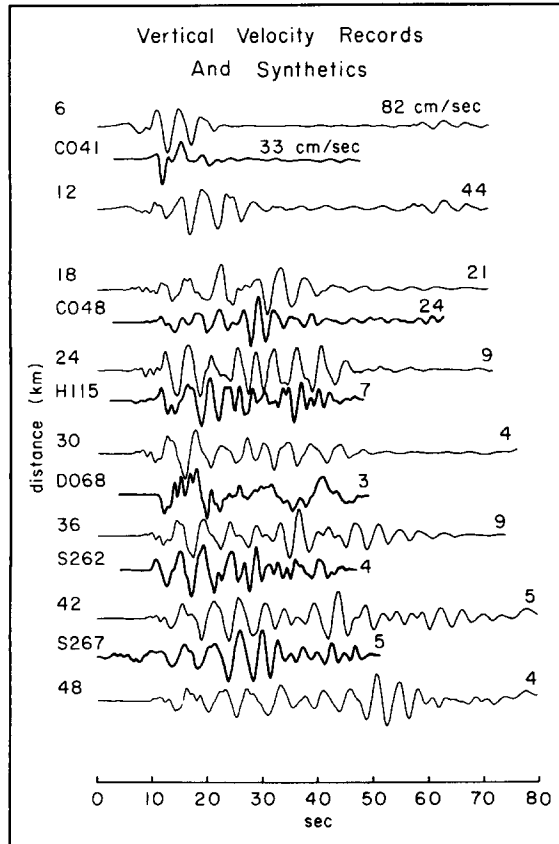
FIG. 11. Comparison of filtered vertical component of data with finite-difference seismograms computed with the empirical time function shown in Figure 8. The heavy traces show the data, with the station name to the *left* and the amplitude in centimeters/second to the *right*. The light traces show the finite-difference seismograms, with the range in kilometers to the *left* and the amplitude to the *right*. The data are lined up on a high-frequency arrival on the vertical component that is presumably a direct compressional wave. The finite-difference seismograms assume a point source at the location D (10 km depth) in Figure 3; they are computed with the structure shown in Figure 3, and a Q of 25 is assumed. The amplitudes of the finite-difference seismograms are consistent with those for the transverse component in Figure 9.

Two troublesome problems appear in the forward modeling of the San Fernando records. First, the small amount of shallow moment release allowed by our model is in conflict with observations of 1 m of thrust motion measured at the surface by Alewine (1974), as well as the suggestions of Alewine (1974), Langston (1978), and Heaton (1982) of significant shallow moment release. In our model, sources at between 6 and 14 km depths excite basins in a similar way, so it is only in the top 5 km that we would exclude significant moment release. The layered model of Langston (1978) and the half-space model of Heaton (1982) overestimate the velocity near the surface, so a smaller moment would serve to excite the same energy in the seismic waves given the correct lower velocities. Also, it is possible that the energy radiated from the shallow portion of the fault is absorbed by some mechanism such as decoupling of the two sides of the fault plane or very low Q in the region, but these explanations are not compelling. The main point of this paper is that the relative amplitudes and duration of shaking across basins can be explained with finite-difference modeling, and the details of faulting in our model are secondary.
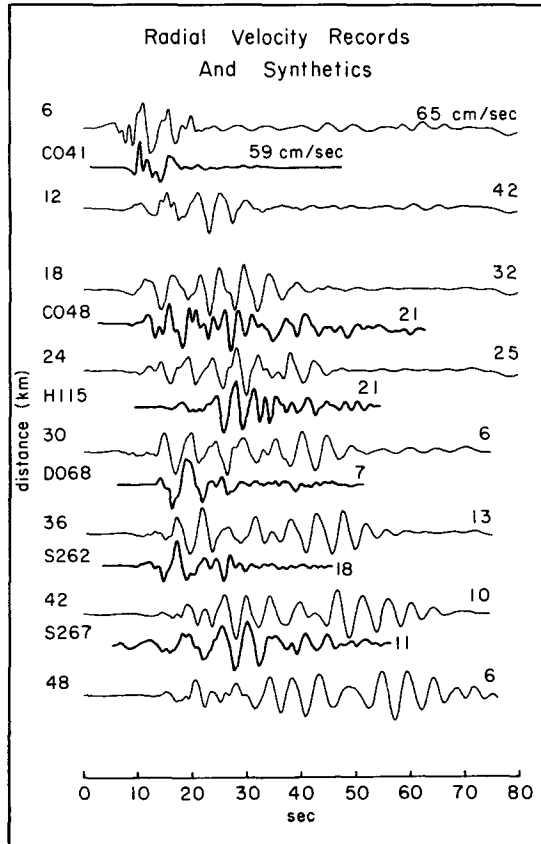
FIG. 12. Comparison of filtered radial component of the data with finite-difference seismograms computed with the empirical time function shown in Figure 8. The heavy traces show the data, with the station name to the *left* and the amplitude in centimeters/second to the *right*. The light traces show the finite-difference seismograms, with the range in kilometers to the *left* and the amplitude to the *right*. The data are lined up on a high-frequency arrival on the vertical component that is presumably a direct compressional wave. The finite-difference seismograms assume a point source at the location D (10 km depth) in Figure 3; they are computed with the structure shown in Figure 3, and a Q of 25 is assumed. The amplitudes of the finite-difference seismograms are consistent with those for the transverse component in Figure 9.

To the extent that shallow sources tend to excite larger motions in the San Fernando basin relative to those in the Los Angeles basin than were observed, this study suggests less moment release shallower than about 6 km depth than the studies of Langston (1978) and Heaton (1982).

The second problem may be seen in Figures 11 and 12, where the Rayleigh wave created in the San Fernando basin tunnels across the Santa Monica Mountains and has a much larger amplitude in the Los Angeles basin than is seen in the data. We have tried rather extreme structures such as more separation between the basins and different kinds of edges on the basins, but the Rayleigh waves simply are better at tunneling across the mountains than are the Love waves, and it is difficult to match the data. Three-dimensional effects may be responsible for this problem. Since this profile skirts the west edge of the Los Angeles basin, the Rayleigh waves jumping the mountains will be refracted into the slower material in the center of the basin, and the amplitude of these Rayleigh waves at stations H118 and S267 may be small.

An alternative explanation may be that the velocity model for the San Fernando basin has too thick a column of slow sediments. In the data, it appears that the surface waves are shorter period in the San Fernando than the Los Angeles basin. In the model, the same 3- to 5-sec period surface waves are excited in both the San Fernando and Los Angeles basins, suggesting that the San Fernando basin model is inaccurate, in that it should have a thinner layer of slow sediments than the Los Angeles basin. If the two basins had distinctly different resonant periods, the surface waves from the San Fernando basin would not excite the Los Angeles basin as much.

The peak amplitude comparison between the data and the finite-difference synthetics is summarized in Figure 13. The match is very good. We did not deviate from the velocity model derived from Duke *et al.* (1971) to keep this as much of a forward-modeling exercise as possible. We feel as a forward-modeling exercise, this simulation has been successful.

For insight into the creation and destruction of the surface waves at the edges of the basins, the envelope of the transverse velocity records is shown in Figure 14. For this plot, 250 rather than eight receivers are used. In this figure, a sketch of the basins and mountains is included at the bottom for location. We use the same source location and empirical time function as we did for the previous synthetics seismograms. The first arrival in the seismograms displayed in Figures 9 and 14 is the direct *SH* wave. The direct wave advances slightly at the Santa Monica Mountains because of the faster material at the surface. In both the San Fernando and the Los Angeles basins, the direct *SH* wave incident upon the edge of the basin nearest the epicenter produces a surface wave train (Love waves) that crosses the basin then converts back to body waves.

Some energy from the Love wave in the San Fernando basin converts to a body wave, with a rapid apparent velocity across the Santa Monica Mountains, then
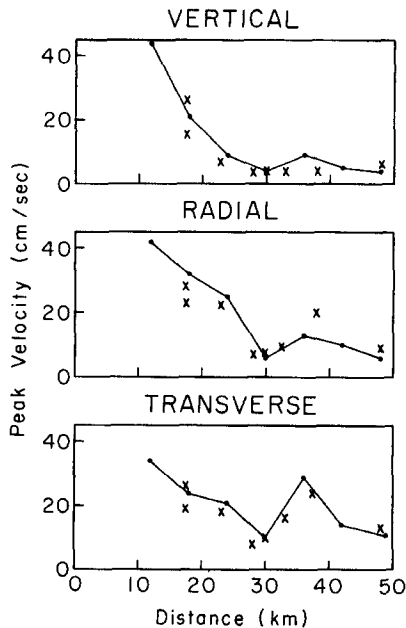

FIG. 13. Peak velocity attenuation with distance. The crosses show the peak velocity of the smoothed data versus offset. The line shows the attenuation for the finite-difference simulation of the motions.
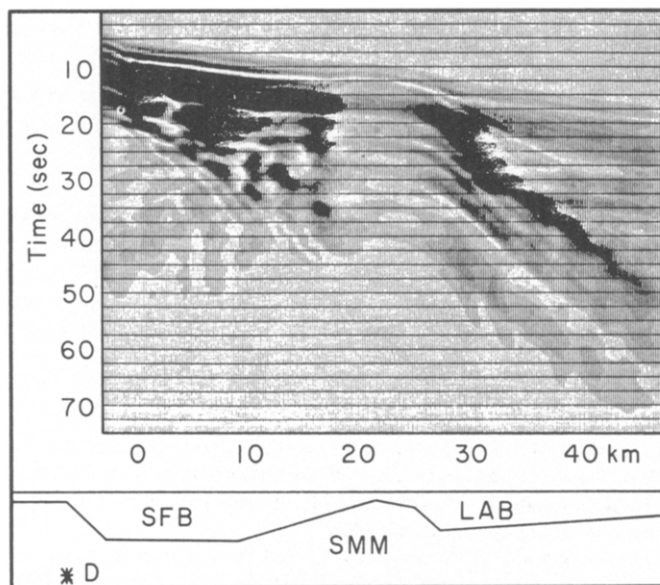
FIG. 14. A seismic section of the envelope of the transverse component of velocity across the San Fernando and Los Angeles basins. Dark portions of the images have energy in the velocity traces; light portions have little or no energy at that time. Two hundred fifty receivers are used, rather than the eight shown up to this point. The same source is used as in Figure 8. The major geologic structures are sketched below the section, where SFB indicates the San Fernando basin, SMM the Santa Monica Mountains, and LAB the Los Angeles basin.

partially converts back to a surface wave in the Los Angeles basin. This arrival may be thought of as surface-wave energy that has tunneled across the mountains. The surface wave generated by the direct *SH* pulse, however, is stronger than the tunneling surface wave for this source location and mechanism.

CONCLUSIONS

The strong motions recorded within the San Fernando and Los Angeles basins during the San Fernando earthquake of 1971 can be largely understood by forward modeling with teleseismically determined source parameters through known structure with only two-dimensional variations in velocity and density. This modeling will accept less moment release shallower than 5 km depth than has been suggested in some previous studies, but this inconsistency might be reconciled if the fully three-dimensional structure appropriate for closed basins is used in the finite-difference calculation. The dramatic differences between using the laterally varying structure of Duke *et al.* (1971) and a flat-layered structure render it impossible to fit this data from the San Fernando earthquake with a flat-layered model.

The geometry of the basin structure is important in determining the attenuation of peak velocity along a profile, as has been previously suggested by theoretical studies (Boore, 1970; Lysmer and Drake, 1972; Bard and Gariel, 1986). The mountains shadow the basins behind them against shallow surface waves, but the edges of the basin nearest the earthquake tend to convert body waves again to shallow surface waves. The source depth of the earthquake is less important for the flat-layered case in determining the duration of shaking and attenuation of peak amplitude with distance. Basins with sharp edges tend to generate some back-scattered surface waves; basins with gradual edges have negligible back-scattered energy.

It is encouraging that the 2- to 10-sec period seismic waves observed in the San Fernando and Los Angeles basins can be largely explained by known structure. We feel that this line of deterministic modeling can help us understand and reduce the uncertainties in amplitude attenuation with distance of strong motions.

ACKNOWLEDGMENTS

REFERENCES

Alewine, R. W., III (1974). Application of linear inversion theory toward the estimation of seismic source parameters, *Ph.D. Thesis*, California Institute of Technology, Pasadena, California, 303 pp.

Alford, R. M., K. R. Kelley, and D. M. Boore (1974). Accuracy of finite-difference modeling of the acoustic wave equation, *Geophysics* **39**, 834–842.

Allen, C. R., T. C. Hanks, and J. H. Whitcomb (1973). San Fernando earthquake: seismological studies and their implications, in *San Fernando, California, Earthquake of February 9, 1971*, Vol. 1, *Geological and Geophysical Studies*, U.S. Government Printing Office, Washington, D.C.

Alterman, Z. and F. C. Karal (1968). Propagations of elastic waves in layered media by finite-difference methods, *Bull. Seism. Soc. Am.* **58**, 367–398.

Bard, P. and J. Gariel (1986). The seismic response of two-dimensional sedimentary deposits with large vertical velocity gradients, *Bull. Seism. Soc. Am.* **76**, 343–366.

Boore, D. M. (1970). Love waves in a non-uniform waveguide: finite difference calculation, *J. Geophys. Res.* **75**, 1512–1527.

Carpenter, E. W. (1967). Teleseismic signals calculated for underground, underwater, and atmospheric explosions, *Geophysics* **32**, 17–32.

Day, S. M. and J. B. Minster (1984). Numerical simulation of attenuated wavefields using a Pade approximant method, *Geophys. J. R. Astr. Soc.* **78**, 105–118.

Drake, L. A. and A. K. Mal (1972). Love and Rayleigh waves in the San Fernando Valley, *Bull. Seism. Soc. Am.* **62**, 1673–1690.

Duke, C. M., J. A. Johnson, Y. Kharraz, K. W. Campbell, and N. A. Malpiede (1971). Subsurface site conditions and geology in the San Fernando earthquake area, UCLA-ENG-7206, School of Engineering, UCLA, Los Angeles, California.

EERL, Caltech (1974). *Strong Motion Earthquake Accelerograms*, vol. II, Report from Earthquake Engineering Research Laboratory, California Institute of Technology, Pasadena, California.

Futterman, W. I. (1962). Dispersive body waves, *J. Geophys. Res.* **67**, 5279–5291.

Hanks, T. C. (1975). Strong ground motion of the San Fernando, California, earthquake: ground displacements, *Bull. Seism. Soc. Am.* **65**, 193–225.

Heaton, T. H. (1982). The 1971 San Fernando earthquake: a double event?, *Bull. Seism. Soc. Am.* **72**, 2037–2062.

Helmberger, D. H. and J. E. Vidale (1988). Modeling strong motions produced by earthquakes with two-dimensional numerical codes, *Bull. Seism. Soc. Am.* **78**, 109–121.

Kanamori, H. and D. Hadley (1975). Crustal structure and temporal velocity change in southern California, *Pageoph* **113**, 257–280.

Langston, C. A. (1978). The February 9, 1971 San Fernando earthquake: a study of source finiteness in teleseismic body waves, *Bull. Seism. Soc. Am.* **68**, 1–29.

Liu, H. L. and T. H. Heaton (1984). Array analysis of the ground velocities and accelerations from the 1971 San Fernando California earthquake, *Bull. Seism. Soc. Am.* **74**, 1951–1968.

Lysmer, J. and L. A. Drake (1972). A finite element method for seismology, in *Methods of Computational Physics*, vol. 11, Bruce Bolt, Editor (entitled *Seismology: Surface Waves and Earth Oscillations*).

McCowan, D. W., P. Glover, and S. S. Alexander (1977). A static and dynamic finite element analysis of the 1971 San Fernando, California, earthquake, *Geophys. J. R. Astr. Soc.* **48**, 163–185.

Montalbetti, J. F. and E. R. Kanasewich (1970). Enhancement of teleseismic body phases with a polarization filter, *Geophys. J. R. Astr. Soc.* **21**, 119–129.

Vidale, J. E. (1986). Complex polarization analysis of particle motion, *Bull. Seism. Soc. Am.* **76**, 1393–1405.

Vidale, J. E. and R. W. Clayton (1986). A stable free-surface boundary condition for 2-D elastic finite-difference wave simulation, *Geophysics* (in press).

Vidale, J. E. and D. H. Helmberger (1987). Path effects in strong motion seismology, in *Methods of Computational Physics*, vol. 11, Bruce Bolt, Editor (entitled *Seismic Strong Motion Synthetics*).

Vidale, J. E., D. H. Helmberger, and R. W. Clayton (1985). Finite-difference seismograms for *SH* waves, *Bull. Seism. Soc. Am.* **75,** 1765-1782.

Whitcomb, J. H., C. R. Allen, J. D. Garmany, and J. A. Hileman (1973). San Fernando earthquake series, 1971: focal mechanisms and tectonics, *Rev. Geophys. Space Phys.* **11,** 693-730.

Witte, D. and P. G. Richards (1986). Anelastic wave propagation by the pseudo-spectral method, *EOS, Trans. Am. Geophys. Union* **67,** 303.

SEISMOLOGY LABORATORY
CALIFORNIA INSTITUTE OF TECHNOLOGY
PASADENA, CALIFORNIA 91125
CONTRIBUTION NO. 4360